Ultra-High-Resolution 3D Optical Coherence Tomography Reveals Inner Structures of Human Placenta-Derived Trophoblast Organoids

Abigail J. Deloria, Sandra Haider, Bianca Dietrich, Victoria Kunihs, Simon Oberhofer, Martin Knöfler, Rainer Leitgeb, Mengyang Liu, Wolfgang Drexler, and Richard Haindl

Abstract*—*Objective: **3D optical coherence tomography (OCT) is used for analyses of human placenta organoids *in situ* without sample preparation. *Methods:* The trophoblast organoids analyzed were derived from primary human trophoblast. In this study a custom made ultra-high-resolution spectral domain OCT system with uniform spatial and axial resolution of 2.48 μm in organoid tissue was used. The obtained OCT results align to differentiation status tested *via* quantitative polymerase chain reaction, Western blot analyses, immunohistochemistry, and immunofluorescence of histological sections. *Results:* 3D OCT enables a more detailed placenta organoid monitoring compared to brightfield microscopy. Inner architecture with light scattering "bridges" surrounding cavities were visualized and quantified *in situ* for the first time. The formation of these bridges and cavities is congruent to differentiated trophoblast organoids having developed syncytiotrophoblasts. *Conclusion:* Using 3D OCT in living placenta organoids is a fast tool to assess the differentiation status and resolve internal structures *in situ*, which is not possible with standard live cell imaging modality. *Significance:* Only recently human placenta-derived organoids were established, allowing to have a highly reproducible and stable *in vitro* model to investigate not only developmental but also physiological and pathophysiological processes during early pregnancy. To our knowledge, this work is the first to analyze living human placenta organoids using 3D OCT. Thereby, the rapid and especially non-endpoint OCT qualitative analyses align to the differentiation stage of organoids, which will aid future advancement in this field.**

***Index Terms*—Image acquisition, optical coherence tomography, organoid, placenta, trophoblast.**

Manuscript received August 17, 2020; revised October 21, 2020; accepted November 9, 2020. Date of publication November 17, 2020; date of current version July 19, 2021. This work was supported in part by Joint PhD Program Medical University of Vienna / NTU Singapore "Kooperation Singapur" (SO10300010), in part by European Commission Horizon 2020 LEIT Information and Communication Technologies under Grant agreement No. 688173 (OCTCHIP) and No. 732720 (ESOTRAC). *(A. J. Deloria and S. Haider contributed equally to this work.) (Corresponding author: Richard Haindl.)*

Abigail J. Deloria, Simon Oberhofer, Rainer Leitgeb, Mengyang Liu, and Wolfgang Drexler are with the Center for Medical Physics and Biomedical Engineering, Medical University of Vienna.

Sandra Haider, Bianca Dietrich, Victoria Kunihs, and Martin Knöfler are with the Department of Obstetrics and Gynaecology, Medical University of Vienna.

Richard Haindl is with the Center for Medical Physics and Biomedical Engineering, Medical University of Vienna, Vienna 1090, Austria (e-mail: richard.haindl@meduniwien.ac.at).

This article has supplementary downloadable material available at https://doi.org/10.1109/TBME.2020.3038466, provided by the authors.

Digital Object Identifier 10.1109/TBME.2020.3038466

I. Introduction

CELL culture is an indispensable preclinical model system to study physiological events, disease, and drug discovery. Conventionally, 2D cell culture are used in which cells adhere in a monolayer to the flat surface of a petri dish [1], [2]. However, cells in the body interact in a 3D microenvironment which influences cellular proliferation, differentiation, and function due to different signals, chemical gradients, and cell-cell interactions [1], [3]. 3D cell culture, such as spheroids and organoids, have been developed to address these shortcomings [1], [3]. The former is a simple form of aggregated cellular spheres, often derived from epithelial cancers and maintained as free-floating cultures [4]. In contrast, organoids are formed by stem or progenitor cells, that give rise to complex, self-organizing, and self-renewing 3D cell culture systems embedded in a matrix-gel recapitulating more closely features of *in vivo* organs [5]–[7]. Another advantage of organoids is their amenability for genetic manipulation, monitoring, and molecular assays compared to *in vivo* models [8]. A plethora of organoids of different organs were already established such as brain, breast, liver, colon, and pancreas [9]. Recently, self-renewing placenta organoids, derived from isolated trophoblasts of first trimester placentae, were developed and are used as a model system for the early human placenta [10], [11]. These works set the fundament to elucidate physiological and pathophysiological processes aiming for placental disease modeling and fetal-maternal interaction during placentation. The human placenta is an extraembryonic organ and connects the mother to the fetus. Beside the exchange of nutrients and gases, the placenta produces pregnancy hormones, such as human chorion gonadotropin (hCG) required for the establishment and maintenance of pregnancy, and specified placental cells effectuate the maternal acceptance of the fetal allograft. Failures in placentation result in gestational disorders such as preeclampsia, intra-uterine growth restriction and recurrent abortion. In the first trimester of pregnancy, the human placenta has a tree-like (villous) structure that is composed of a stromal part being covered by a bi-layer of the so-called trophoblasts. Villous cytotrophoblast (vCTBs), directly contacting the stroma, undergo two differentiation routes. Firstly, vCTBs proliferate and fuse

into the overlying syncytiotrophoblast (STB) layer, which is responsible for hormone production and transport functions. Secondly, intensive proliferation of vCTBs at villous tips lead to the generation of extravillous trophoblasts that invade maternal uterine tissues to transform maternal vessels, thereby providing an adequate blood flow to the fetus during the gestation, and to adapt the maternal immune system to the fetal semi-allograft [10]. However, the current understanding of the first weeks of human placentation were mainly derived from interpretations of hysterectomy specimen as well as studies in mice and great apes [12], [13]. 2D trophoblastic cell lines as well as 2D human primary trophoblasts isolated from first-trimester placentae were developed [14], but are not an adequate model as they rapidly terminate proliferation and differentiate *in vitro*. Further, they do not properly represent 3D *in vivo* morphology and cell composition [4]. In the last three years, the establishment of human trophoblast stem cells [15], and especially trophoblast organoids [10], [11] have substantially improved the field of placental research. Trophoblast organoids (TB-ORGs) are densely packed, consisting of an outer cell layer of proliferative vCTBs which differentiate into hormone-producing STBs toward the center of organoids. However, most imaging analyses were conducted as endpoint studies in which the organoid cultures were fixed and processed for either immunofluorescence analyses or electron transmission microscopy [10], [11]. Longitudinal studies monitoring living organoids were performed by phase contrast/brightfield imaging, but due to the shallow penetration depth in large organoids (300 to 800 μm), their inner structures were neither clearly discernible nor quantifiable [10], [11]. Moreover, the above-mentioned endpoint analyses require the termination of the experiment at potentially suboptimal time points [16]. Additionally, the inevitable fixation and clearing procedures cause alterations in 3D structures such as shrinking and collapsing of organoids [17], and cross sections are only snapshots of individual organoids [16]. Indeed, serial cross section staining and fluorescence Z-Stack images of the whole organoid can be obtained, but inherently do not eliminate the need of genetic fluorescent reporters or extensive sample preparation [17].

In organoid cultures such as organoids of the brain [18] or colon [17], light sheet and multiphoton imaging were used for volumetric imaging. Here, entire organoids can be imaged in detail, but fixation, labeling, and optical clearance need to be performed [17]. Further, micro-computed tomography (microCT) was established for analyzing dentin-pulp-like and retinal organoids, but again, sample fixation was required [19], [20]. Improvement of live imaging was obtained with lattice light sheet microscopy, but this technique still required fluorescence labeling [21]. Other methods, such as hyperspectral imaging and fluorescence lifetime imaging microscopy allows imaging of the metabolism of organoids without labeling [20], however, these are costly methods and are only providing intensity projections. In contrast, optical coherence tomography (OCT) allows optical sectioning of organoids enabling label free, longitudinal studies. OCT is based on low-coherence interferometry [22] and takes advantage of intrinsic scattering contrast arising from biological tissue due to different refractive indices [23]. OCT has been widely used in several clinical fields including ophthalmology [24] and dermatology [25], but also has started to being used in 3D cell cultures, such as organoids and tumor spheroids [26]–[28]. So far, stem cell-derived organoids of human retinal [16], [20], [29], [30] and intestinal origin [31] were analyzed by OCT.

In this work, we hypothesize that 3D OCT enables to determine the inner structures of living placenta organoids *in situ* without sample preparation and to align the obtained recording to the differentiation status of organoids.

Herein, we will demonstrate that the 3D OCT imaging technology can be used to monitor STB formation in individual TB-ORGs in a volumetric, non-invasive, and non-labelling manner. By using specific inhibitors blocking STB differentiation we provide controls that allow to verify the strong and direct relationship between OCT-obtained imaging data with conventional end-point-derived methods.

II. Methods

A. Trophoblast Organoid Formation and Cultivation

Isolation, utilization of placenta tissue, and all experimental procedures were approved by the ethics board of the Medical University of Vienna (Number 084/2013) requiring informed consent of all patients and are in adherence with the Helsinki Declaration. Human first-trimester placental tissues from 6th to 7th week of gestation (n = 3) were collected from elective pregnancy terminations. Trophoblast organoids were generated and cultivated as described previously [10]. In brief, villous cytotrophoblasts were obtained after sequential digestion of the placental tissue, and embedded in a semi-solid 60% growth factor reduced-matrigel (GFR-M) diluted with organoid growth medium consisting of DMEM/F12 (Invitrogen) supplemented with 1x N2 (Gibco), 1x B27 (Gibco), 2 mM glutamine (Gibco), 10 mM HEPES (Gibco), 1 μM A83-01, 100 ng/ml recombinant human epidermal growth factor (rhEGF, R&D Systems) and 3 μM CHIR99021 (Tocris). Drops (40 μl) of cell-GFR-M mixtures were placed in the center of 4-well dishes (Nunclon Delta Surface, Thermo Scientific) and incubated for 1 minute at 37 °C and 5% CO_2 in a humidified incubator. Subsequently, plates were flipped upside down and incubated for another 15 minutes to ensure equal distribution of the cells in the solidifying GFR-M drops. Afterwards, the plates were flipped back and 0.5 ml of organoid growth medium was added to the dishes. After 7 to 10 days, TB-ORGs were split and treated with or without 10 μM p38 MAPK inhibitors (SB202190, Stemcell Technologies). The culture medium was changed every 2 to 4 days. After additional 10 days of cultivation, brightfield images were taken with the EVOS FL Cell Imaging System microscope (Life technologies) and OCT images were obtained. Next, organoids were either fixed for immunofluorescence analyses or harvested for ribonucleic acid (RNA) and protein isolation.

B. Optical Coherence Tomography System Set-Up

In the customized 3D bulk-optics spectral domain OCT we used a novel polarization-aligned three SLED broadband source

(EBD290002-00, EXALOS AG) with a central wavelength of 846 nm and a 3 dB bandwidth of 133.3 nm [32]. The spectrometer for measuring the interference signals between the sample and the reference arm comprised a transmitting diffraction grating (3253-W-01, Wasatch Photonics), a lens system (85 mm f/2.0 Makro-Planar T, Zeiss) and a Basler Sprint spL4096-140km line scan camera. The sample arm applied galvanometer scanners (CTI6220H, Cambridge Technology), a 4 focal length lens system and an Olympus-UPlanSApo 4 telecentric microscope objective to perform raster scanning across the sample with an axial resolution of 3.40 μm in air. A refractive index of 1. 37 [33], similar to cancer spheroids, was assumed for quantitative axial measurements and 3D reconstructions, leading to an axial resolution of 2.48 μm in tissue. The transverse resolution was measured to be 2.48 μm. The transverse pixel step size was 1.27 μm. The optical power at the sample was approximately 500 μW for all experiments.

C. OCT Data Acquisition and Reconstruction

For OCT imaging, the 4-well plates with the living organoids were placed in focus on the sample holder of the OCT system and tilted by 10° to prevent back reflection from the cell culture dish. OCT images were acquired with 5 kHz line rate and depending on the size of the organoid 200 to 800 A-scans per 200 to 800 B-scans were acquired. The obtained OCT interferogram was subjected to standard OCT signal processing (background subtraction, dispersion compensation, zero-padding interpolation, fast Fourier transform) [34]. For visualization, the imaging software ImageJ 1.52p (Wayne Rasband, National Institutes of Health, USA) was used for 2D images and Icy 2.0.3.0 (BioImage Analysis unit Institut Pasteur) for 3D rendering, respectively. ImageJ was used for semi-automated quantification of the organoids.

D. Immunofluorescence and H&E Staining

After imaging of the placenta organoid with OCT the samples were subjected to fixation, paraffin embedding, hematoxylin and eosin (H&E), and immunofluorescence staining as previously described [10]. In brief, organoid domes were washed with phosphate-buffered saline (PBS) and fixed in 4% formaldehyde solution (Honeywell) overnight at 4 °C. Afterwards, the organoids were washed with PBS twice, and incubated for 30 minutes with 70% ethanol (EtOH) supplemented with 10 μl alcian blue (Merck) to enhance visibility. Next, the samples were dehydrated with rising concentrations of EtOH and lastly with xylene, 15 minutes each at room temperature (RT). Subsequently, samples were impregnated in pre-warmed paraffin (Histowax) at 65 °C and then allowed to solidify on an ice-cold plate. Serial sections (2 to 3 μm) were deparaffinized, rehydrated and either stained with H&E using standard procedures [35], [36], or immunofluorescence was performed. For the latter, antigen retrieval was done with 1x PT module buffer 1 (100x stock solution, Thermo Scientific) for 35 minutes at 93 °C using a KOS microwave histostation (Milestone). Then, sections were incubated with blocking solution (PBS/0.5% fetal bovine serum/0.3% Triton X-100) for one hour at RT. Afterwards, slides were incubated with primary antibodies for staining the protein of interests (diluted in PBS/1% Bovine Serum Albumin/0.3% Triton X-100) at 4 °C overnight. The following antibodies were used: rabbit polyclonal anti-SDC1 (Sigma, Cat. No. HPA006185, 1:200), mouse monoclonal anti-E-cadherin (BD Transduction Laboratories, Cat. No. 610181, 1:200). Next, the slides were washed three times with PBS and incubated with appropriate secondary antibodies (2 μg/ml; Alexa, Molecular Probes) for one hour at RT. Nuclei were stained with 1 μg/ml 4′,6-Diamidino-2-phenylindole dihydrochloride (DAPI, Roche) and sections were embedded using fluoromount G (Soubio). Stained sections were analyzed by fluorescence microscopy (Olympus, BX50) and digitally photographed (CellP software, Olympus).

E. RNA Isolation and Quantitative PCR

For RNA isolation, organoid samples were washed with ice-cold PBS and the Matrigel was dissolved with cell recovery solution (Corning) at 4 °C for 45 minutes. The organoids were then homogenized using the Precellys 24 (PeqLab) with CK-Mix tubes and Tri-Reagent (PeqLab), and RNA isolation was performed as instructed by the manufacturer. RNA (1 μg each) was reverse-transcribed (RevertAid H Minus Reverse Transcriptase, Fermentas) according to the manufacturer's instructions. qPCR analyses were performed using the 7500 Fast Real-time PCR System (Applied Biosystems, ABI) as described by using the TaqMan Gene expression assays for *ENDOU* (ABI, Hs00195731-M1) and *CGβ* (ABI, Hs00361224_g) [37]. Per sample, 1 μl copy deoxyribonucleic acid (cDNA), 0.5 μl primers, 5 μl innuMIX qPCR MasterMix Probe (Biometra) and 0.3 μl ROX reference Dye (Invitrogen) were used and signals (Δct) were normalized to TATA-box binding protein (TBP, ABI, 4333769F).

F. Western Blot

Whole protein lysates were obtained after RNA isolation using Tri-Reagent (PeqLab) as instructed by the manufacturer. Protein extracts were separated on sodium dodecyl sulfate/polyacrylamide gels, transferred onto polyvinylidene difluoride membranes (GE Healthcare), and incubated overnight at 4 °C with the following primary antibodies: rabbit polyclonal anti-Poly (U)-specific endoribonuclease (ENDOU) (Sigma, Cat. No. HAP012388, 1:1000); rabbit polyclonal anti-human chorionic gonadotropin (CGβ, Dako, Cat. No. A0231, 1:500) and rabbit monoclonal anti-glyceraldehyde-3-phosphate dehydrogenase (GAPDH, Cell signaling Cat. No. 2118, 1:5000). Afterwards, filters were washed three times with tris-buffered saline (TBS) containing 0.1% Triton X-100 (TBS-T) and incubated with goat anti-rabbit horseradish peroxidase (HRP)-conjugated antibodies (Cell signaling, Cat. No 7074, 1:10000) for one hour at room temperature. Membranes were washed again with TBS-T three times and signals were developed using Western Bright Chemiluminescence Substrat Quantum (Advansta) and visualized with ChemiDoc Imaging System (Bio-Rad) using Image Lab 6.0 software.

G. Manual Segmentation for OCT vs Brightfield Comparison and Statistical Analysis

ImageJ was used to quantify the area of organoids. Thereby, the organoid was circumvented and the region of interest (ROI) saved in ImageJ ROI manager. For processing brightfield images, the length of the incorporated scale bar was used to set the correct distance in pixels to obtain the area of the circumvented organoid. For OCT images, the scale was set to 0.79 pixels/μm based on the pixel step size.

For comparing brightfield and OCT microscopy nine organoids were measured three times *via* ImageJ by three raters on OCT and brightfield images. To test interrater reliability intraclass correlation coefficient (ICC) estimates and their 95% confidence intervals were calculated based on 2-way mixed-effects model, mean-rating (k = 3), absolute-agreement. As basis for evaluating the level of reliability 95% confidence interval of the ICC estimate was used: Values less than 0.50 were indicative of poor reliability, values 0.50 to 0.75 moderate reliability, 0.75 to 0.90 good reliability, and values greater than 0.90 excellent reliability according to Koo and Li [38]. For comparing brightfield and OCT images paired t-test was used, thereby p-values smaller than 0.05 were considered as significantly different. Furthermore, a Bland-Altman plot was generated to visualize the agreement [39]. Thereby, the area of the OCT *en face* images were subtracted from the brightfield images to measure the difference. The regression linear coefficient was calculated to test for proportional bias. For obtaining the volume of the whole organoids (n = 4) and their cavities, each OCT cross-sectional segmented area was multiplied by the z-axis pixel size (1.27 μm) and added together. The cavity volume was calculated as percentage with respect to the organoid whole volume (100%).

Statistical analyses were run on IBM SPSS Statistics for Windows, Version 25.0. Armonk, NY: IBM Corp.

III. Results

A. OCT Imaging of TB-ORG Enables Non-Invasive, Detailed Evaluation of Inner Organoid Structures

TB-ORG cultures (n = 3 donors) were used to investigate if OCT provides advantages over standard imaging methods for 3D cell culture. We compared the images of the same living, in GRFM embedded TB-ORGs *via* two *in situ* imaging techniques, brightfield microscopy using the EVOS FL Cell Imaging System microscope (Fig. 1a) and a customized OCT system (Fig. 1b–d), respectively. A tread was used as a marker for orientation and facilitated locating identical organoids in the cell culture well for imaging. Fig. 1a illustrates two representative TB-ORGs. Compared to OCT, the brightfield microscope images revealed only limited structural detail (Fig. 1a). Using OCT, a volume scan enables different organoid assessments and visualization (Fig. 1b–1d), such as *en face* averaged images (Fig. 1b) similar to brightfield images and different cross sections (Fig. 1c). To investigate wether OCT and brightfield imaging techniques were in quantitative agreement, TB-ORG areas of brightfield and *en face* avaraged OCT images of 9 organoids were measured *via* ImageJ by three raters three times and compared. The average measurements of brightfield images and OCT showed no significant difference (p-value = 0.621) when tested with paired samples t-test. To analyse interrater reliability, ICC of the raters were performed. The interrater reliability for raters for brightfield and OCT images were reported as excellent (brightfield ICC = 0.999 with 95% confidence inveral = 0.996 - 1.000; OCT ICC = 0.999 with 95% confidence inveral = 0.996 - 1.000). To assess the agreement between the two microscopy methods, a Bland-Altman plot was generated (Fig. 2). It visualizes the different sized organoids ranging from approximately 5000 μm^2

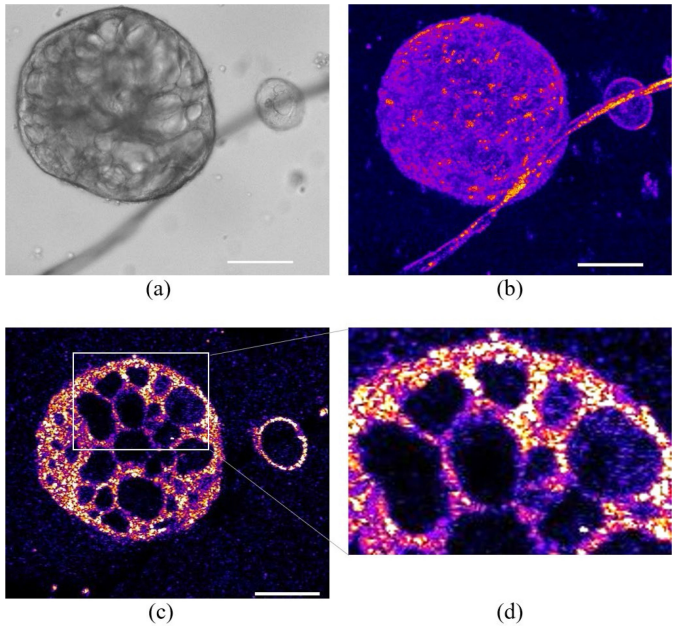

Fig. 1. OCT imaging of TB-ORGs provided additional structural information. The same TB-ORGs embedded in Matrigel were imaged with (a) brightfield microscopy and (b)–(d) OCT. (b) Shows en face averaged, (c) en face single cross section (d) enlarged section marked in c. Representative TB-ORG are depicted. All scale bars 100 μm.

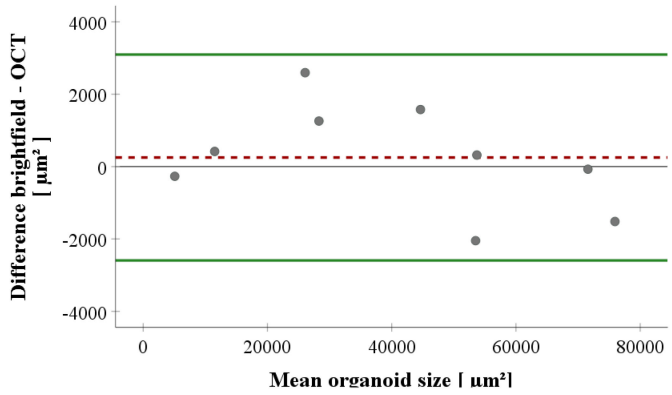

Fig. 2. Bland-Altman plot comparing agreement between brightfield and OCT imaging of TB-ORG: Red dotted line indicates mean of the same TB-ORG (n=9) imaged via brightfield and OCT and subsequently segmented by three raters. Green line shows 95% confidence interval limit, grey line indicates 0 difference between OCT and brightfield measurement.

to 77000 μm^2. The average difference (=250.67 μm^2) of the quantified brightfield and OCT imaged organoids is shown by the red dotted line, indicating an offset resulting from brightfield images being non significantly bigger than OCT measurements. All analyzed organoids were within the 95% limit of agreement (upper limit: 3095.10 μm^2; lower limit -2593.77 μm^2). No proportional bias was evident when testing linear regression (p-value = 0.237).

Investigating the advantages of OCT to optically dissect the specimen, the smaller TB-ORG in Fig. 1c depicts a high scattering cell border with a lumen, which stands in contrast to the bigger TB-ORG with numerous heterogeneously sized cavities. Interestingly, the zoom-in in Fig. 1d allows to appreciate that cavities were filled to different degrees with light scattering content.

In conclusion, areal quantitative assessment of TB-ORG were similar between the brightfield and OCT imaging methods. However, OCT additionally enables to non-invasively reveal details of inner structures which were not possible *via* brightfield microscopy.

B. OCT Allows Appreciation of Organoid 3D Orientation to Each Other and of Internal Structures

From the *en face* images seen in Fig. 1 exact 3D cavity structures cannot be easily identified. However, analyzing and comparing different planes of TB-ORG (Fig. 3) revealed e.g., an elongated cavity spanning throughout the organoid (Fig. 3a, YX plane). The intersections of the yellow lines mark the same position (the center of the elongated cavity) in all three planes (Fig. 3a–c). The white arrows in Fig. 3a and b denote the marking thread at the same position in different planes, cross section/YX and *en face*/XZ plane, respectively. The XZ plane in Fig. 3b was taken at the height of the horizontal yellow line in Fig. 3a, whereas the cross section of YX plane is at the horizontal line depicted in Fig. 3b. The asterisks in Fig. 3b and c are also showing the marking thread at the side of the organoid. Fig. 3d shows a 3D rendering of the TB-ORGs, demonstrating that the bigger organoid was not round but had a more oval-shaped morphology, and the exact constellation of both TB-ORGs to each other in the Matrigel could be delineated. Fig. 3e (and Supplemental Video 1) is a rendering of the elongated cavity, whose orientation within the organoid can be appreciated in Fig. 3f (and Supplemental Video 2).

Taken together, OCT imaging of living TB-ORGs enables to evaluate morphology and orientation of the organoid as well as cavities within TB-ORGs, further indicating that this technology allows for better visualization and characterization of inner TB-ORG structures compared to standard microscopy.

C. OCT Image Aligns With STB Formation

Literature showed that in TB-ORG, vCTBs differentiate into hormone producing STBs toward the centers of the organoids [5]. We therefore assessed whether the cavities seen in OCT images would align to STB formation in TB-ORG. To provide an adequate differentiation control we treated the organoids with or without p38 mitogen-activated protein kinases (MAPK)

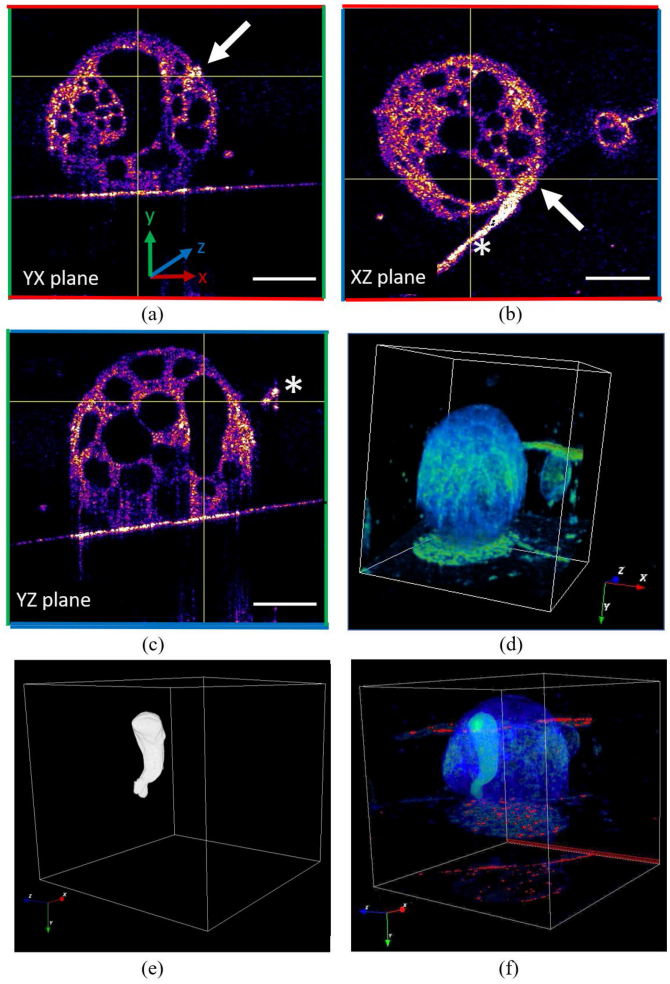

Fig. 3. OCT allows detailed orientational analyses of TB-ORGs. (a)–(c) Orthogonal views of organoids. (d) 3D rendering (e) Isolated longitudinal cavity (f) Cavity highlighted in green within organoid. All scale bars 100 μm. Cube length 500 μm.

signaling inhibitor (Fig. 4). Upon p38 MAPK inhibition, differentiation of STBs, and consequently hormone production, is hampered [40]. Organoids were either treated or not treated (control) with 10 μM p38 inhibitor for 10 days. Then, TB-ORG were imaged without sample preparation with OCT and subsequently either fixed and embedded in paraffin or further processed for RNA as well as protein analyses. Fig. 4 upper panel shows control TB-ORG samples without p38 inhibitor. OCT images and H&E staining revealed the existence of cavities in the central region of the organoids. Immunofluorescence analyses further showed that those cavity structures lack E-cadherin expression and were positive for syndecan-1 (SDC1), two hallmarks of STBs indicating that these cavities indeed recapitulate STB-associated structures [41]. SDC1 further associated well with the high intensity bridges, further confirming that the observed cavities by OCT resembled STB structures. In contrast, p38 inhibitor treated TB-ORG (Fig. 4a, lower panel) failed to show those cavities, in both OCT obtained images and H&E stainings. Immunofluorescence analyses of those samples showed continuous E-cadherin staining throughout the organoid and hardly

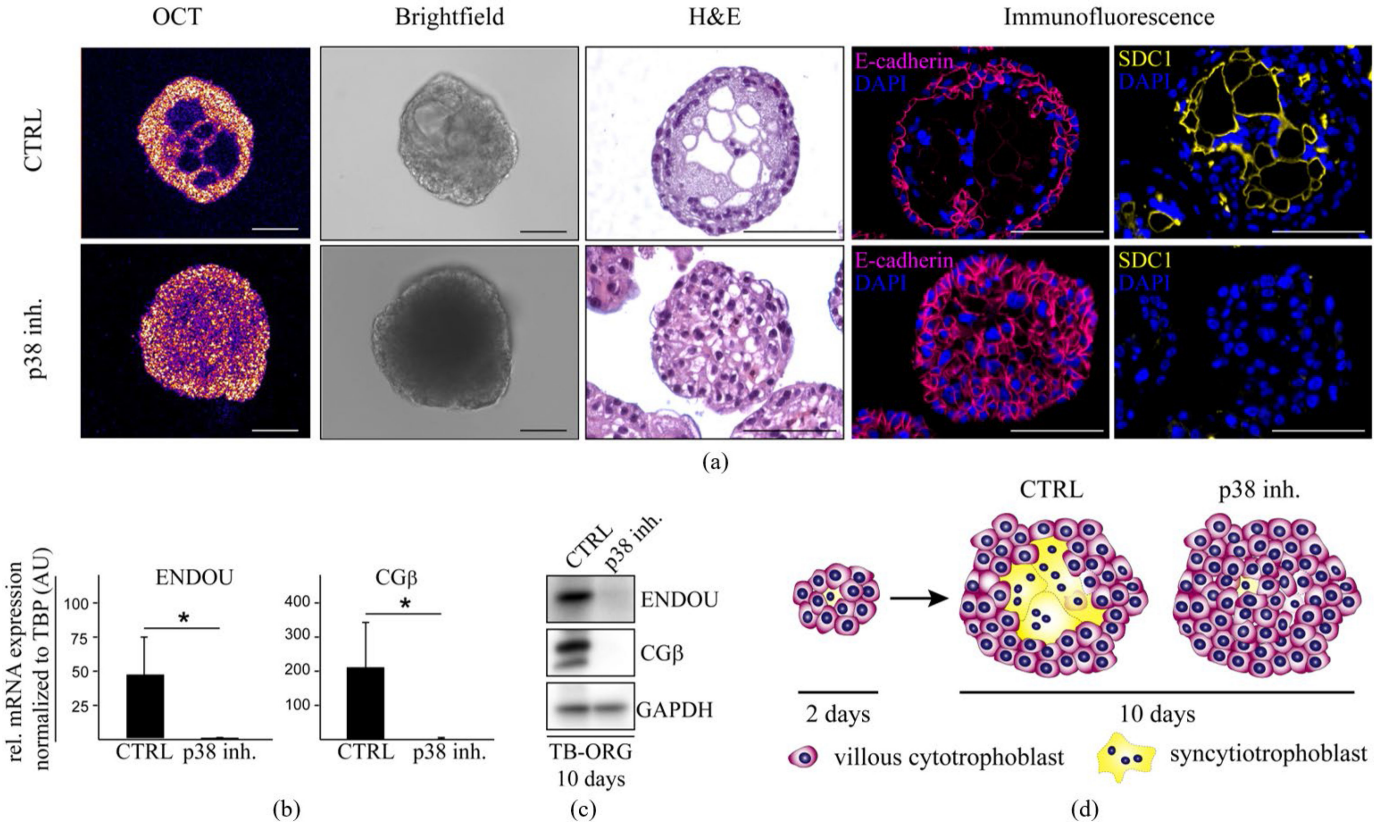

Fig. 4. p38 cell differentiation inhibitor treatment: (a) Comparison between untreated (top column) and treated (bottom column) placenta organoids. (b) qPCR data showing mRNA expression and (c) protein level of ENDOU and CGb in TB-ORG cultures. Mean values +SD (n=3), performed in duplicates and normalized to TBP are shown. $*$ $p<0.05$, AU arbitrary units. (d) Scheme depicting placenta organoid development without and with p38 inhibitor. Scale bars 100 μm.

exhibit SDC1. Consistent with these findings were the results of other syncytiotrophoblast markers on mRNA and protein level (Fig. 4b, c). Western blot and qPCR analyses revealed that the STB marker ENDOU was only detected in the control TB-ORGs.

Further, the pregnancy-specific hormone chorion gonadotrophin β (CGβ) was highly expressed when organoids where not treated with STB differentiation inhibitor and undetectable upon p38 MAPK inhibition (Fig. 4b, c).

In summary, we suggest that the high scattering bridges in the inner part of the TB-ORG represent STB structures and our studies with p38 inhibitor confirmed that OCT images align with the differentiation status of trophoblasts within TB-ORG.

D. Organoid Segmentation Shows Diverse Degree of Differentiation Independent of Size

To enable future longitudinal monitoring and staging of TB-ORGs according to STB and cavity formation, we sought to quantify the volume of the whole organoid and its cavities. Using ImageJ, three raters manually segmented non-treated whole organoids (n = 4) including the cavities or cavities only. Interestingly, placenta organoids exhibited diverse shapes and structures. Fig. 5a–d (Supplemental Video 3) show an irregularly shaped organoid with a large, undifferentiated part and a differentiated, cavity-bearing fraction at the side. To quantify the size of the whole organoid, each TB-ORG cross section was evaluated, thereby the borders of the organoid were circumvented (Fig. 5b). Similarly, each cavity was segmented (Fig. 5c). The cavity in comparison to the whole organoid were calculated in percentage and plotted against the corresponding whole organoid size in Fig. 5e. The analyzed organoids were heterogenous in volume, and irrespective of their size, they bear different percentage range of cavities (TB-ORG1: 8.8 to 10.8%; TB-ORG2: 21.9 to 30.0%; TB-ORG3: 43.1 to 55.1%; TB-ORG4: 41.6 to 52.4%). Of note, TB-ORG3 and TB-ORG4 were the small and big organoids, respectively, displayed in Fig. 1 and Fig. 3. OCT revealed herein that TB-ORGs have heterogenous morphologies and dissimilar differentiation states even within one TB-ORG culture.

IV. Discussion

The human placenta is the connecting organ between the mother and the fetus. Correct placental formation, differentiation, and function display an indispensable pre-requisite for uncomplicated pregnancies. Hence, reliable cell culture models allowing to investigate trophoblast physiology are required. Placenta-derived trophoblast organoids provide a functional experimental model to study not only physiological changes

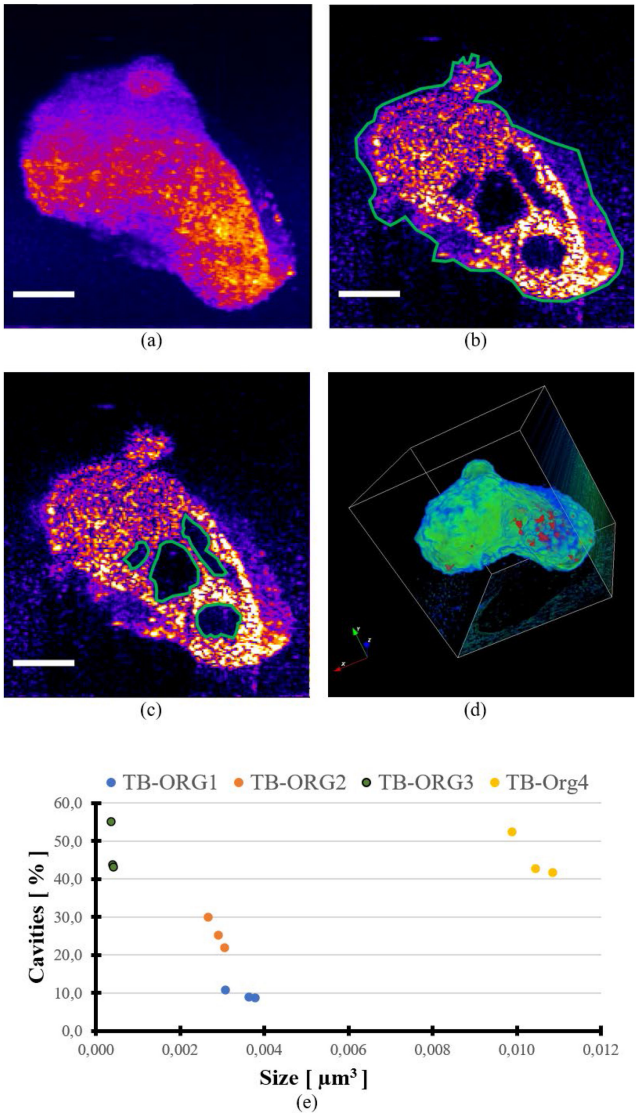

Fig. 5. Example of manual segmentation of TB-ORGs: (a) En face projection. (b) Segmentation region of whole organoid. (c) Cavity segmentation. (d) 3D rendering. (e) TB-ORGs are differently sized and differentiated. Scale bars 50 μm.

in the placenta during early pregnancy, but also to investigate maternal-fetal transmission of drugs, proteins, and pathogens [10], [11]. However, current imaging methods characterizing inner TB-ORG structures – and thus the status of STB formation – require the termination of experiments. Fluorescence imaging methods including light sheet microscopy require exogenous contrast agents for molecular specificity. In contrast, OCT is a label-free and non-invasive volumetric imaging method allowing to assess unperturbed specimen derived from primary tissue. Micro-CT provides deeper imaging penetration than OCT, but requires terminal sample preparation for organoids and has a lower resolution, therefore overlooking morphological features which OCT detects [20]. Serial scanning electron microscopy delivers sub micrometer resolution, however, only thin samples after heavy metal staining, dehydration, and resin-embedding can be imaged.

OCT has e.g., been applied to stem-cell-derived organoids of intestinal and retinal origin [16], [20], [29]–[31]. Retinal layers are aimed to be mimicked in organoids and OCT has been used to investigate their structure *in vitro* and in *in vivo* transplantation studies [20], [29], [30]. Further, intestinal organoids derived from induced pluripotent human stem cells were also characterized *via* OCT. These organoids form a central lumen which does not provide signal and is enclosed by epithelial cells providing the high scattering contrast [31].

However, OCT has not yet been used in trophoblast organoids. Hence, in this work we imaged TB-ORGs of three donors with OCT to determine inner structures and, moreover, align these to the differentiation status of STBs in these organoids.

Therefore, we analyzed placenta organoids with our custom-built spectral domain OCT instrument. Similar to the intestinal organoid lumen [31], cavities in the trophoblast organoids were displayed by no or low OCT signal. In TB-ORG, differentiation of STBs occurs toward the center of organoid structures which is in stark contrast to *in vivo* placental tissue where STBs are on the outside in contact with maternal blood [10]. Nevertheless, encapsulated STBs in trophoblast organoids were functional and secreted the hormone hCG [10], [11]. In this study we demonstrate that the centrally-located differentiated STBs in TB-ORG align to the cavities shown *via* OCT. Since OCT is based on scattering contrast, it is likely that the dark cavities predominantly represent cell-free areas. However, some cavities seem to have scattering properties, a possible indication that they are filled with secreted products of STBs (hormones, transport vesicles) accumulating in the center of organoids [10], [11]. Tang et al. investigated the origin of interference pattern i.e., OCT signal on a subcellular level in glioblastoma cells grown in a semi-solid gel matrix. Thereby, scattering contrast derived from actin filaments, mitochondria, plasma membrane, boundary between cytoplasma and nucleus due to change in refractive index of their lipid, nucleic acid, and protein contents [42]. This was concordant with our results, as OCT scattering was associated to nuclei staining (H&E; DAPI in immune fluorescence) and cellular membrane (E-cadherin, SDC1).

We further tested whether OCT allows to non-invasively determine STB differentiation status in TB-ORGs. In literature, p38 signaling was shown to regulate CTB differentiation to STB, in which mononuclear CTB undergo cell fusion thus forming the syncytium [43], [44]. Therefore, organoids were cultured with the p38 inhibitor SB202190 for 10 days to block trophoblast differentiation and compared to non-treated and therefore differentiated TB-ORGs. The latter showed multinucleated cells towards the center of the organoids, which were positive for the STB membrane marker SDC1 [45]. H&E, immuno stainings and qPCR as well as Western blot analyses revealed that cavities and markers for STB differentiation (CGb, ENDOU, SDC1) were only detectable in non-treated TB-ORGs. These results fit to the images taken by OCT on non-fixed, *in situ* samples during cultivation. Therefore, we conclude that non-invasive, label free OCT enables to qualitatively relate cavity formation to the differentiation of STBs in TB-ORGs.

Additionally, TB-ORG do not only differentiate into STBs but can also be triggered to produce outgrowing extravillous

trophoblasts invading the matrigel. Hence, OCT would also be useful depicting the exact orientation of outgrowing extravillous trophoblasts in 3D [10], [11].

We also investigated the differences between brightfield microscope and OCT images. The Bland-Altman plot is a statistical visualization method assessing agreement between two methods [39]. Here, we analyzed the difference between the images obtained *via* brightfield microscope and OCT compared to the mean organoid size. OCT *en face* averaged TB-ORG images were nonsignificant smaller than when measured with the brightfield microscope. Overall, the Bland-Altman plot and paired samples t-test show the agreement between the two imaging modalities.

TB-ORGs have variable outer and inner morphology which are not resolvable and quantifiable *via* brightfield images. Moreover, as shown in literature, using measured diameter and using the spherical volume formula of 3D cellular structures result in a size overestimation in comparison to voxel-based measurements [33]. In contrast, 3D OCT imaging not only enables to appreciate the volumetric size of the overall organoid, but optical dissection allows to quantify inner structure and cavities of the organoid. Manual segmentation then allowed us to identify differentiation variability in human trophoblast organoids. Similar observation was reported for human retinal organoids [16]. Possible cause may be the requirement of a 3D extracellular matrix which often is the semi-solid gel Matrigel (Corning), which is extracted from mouse sarcoma and therefore is susceptible to batch-to-batch production variation [46]. This may prompt further studies to evaluate possible developmental staging approaches to improve experimental reproducibility. Moreover, the same organoid can be repeatedly imaged over a longer time course. This may bring more insights towards a quantitative link between OCT results and differentiation status. Further, automatic segmentation would be useful for unbiased organoid identification and detailed analyses [47], [48].

V. Conclusion

Our results demonstrate the value of OCT in placenta organoid research. In situ brightfield microscopy only allows to monitor the outer organoid morphology. For characterizations of the inner architecture conventional methods such as H&E and fluorescence staining are used, but are endpoint analyses. In contrast, using OCT enables to visualize and quantify structures which is congruent to the differentiation status of organoids in situ and without sample preparation. These findings will simplify the experimental design and may become an invaluable tool in placental research. Moreover, 3D rendering allows to better appreciate the TB-ORG morphology and orientation, which will also aid further studies focusing on cellular outgrowth of extravillous trophoblasts from the trophoblast organoid. Taken together we suggest that OCT imaging might be routinely included in organoid research to facilitate the monitoring of in situ samples.

Appendix

Supplemental Video 1: 3D cavity

Supplemental Video 2: Cavity within organoid structure

Supplemental Video 3: Cross-section of TB-ORG1

Acknowledgment

The authors would like to thank Marcus Duelk, Stefan Gloor, and Jean Dahdah from Exalos for providing the novel 3-SLED light source; and Christoph Krall as well as Pavla Krotka from the Medical University of Vienna (Center for medical statistics, informatics and intelligent systems) for their assistance during statistical evaluation.

References

[1] K. Duval *et al.*, "Modeling physiological events in 2D vs. 3D cell culture," *Physiol. (Bethesda)*, vol. 32, no. 4, pp. 266–277, Jun. 2017.

[2] R. Edmondson *et al.*, "Three-dimensional cell culture systems and their applications in drug discovery and cell-based biosensors," *Assay Drug Develop. Technol.*, vol. 12, no. 4. Mary Ann Liebert, pp. 207–218, May. 01, 2014.

[3] W. Mueller-Klieser, "Three-dimensional cell cultures: From molecular mechanisms to clinical applications," *Amer. J. Physiol. - Cell Physiol.*, vol. 273, no. 4, pp. 42–44. Am J Physiol, 1997.

[4] L. B. Weiswald *et al.*, "Spherical cancer models in tumor biology," *Neoplasia (United States)*, vol. 17, no. 1. Neoplasia Press, Inc., pp. 1–15, Jan., 2015.

[5] "An update on organoid research Ed.ial," *Nat. Cell Biol.*, vol. 20, no. 6, p. 633, Jun. 01, 2018.

[6] M. Simian and M. J. Bissell, "Organoids: A historical perspective of thinking in three dimensions," *J. Cell Biol.*, vol. 216, no. 1, pp. 31–40, 2017.

[7] G. Rossi *et al.*, "Progress and potential in organoid research," *Nat. Rev. Genet.*, vol. 19, no. 11. Nature Publishing Group, pp. 671–687, Nov., 2018.

[8] A. Fatehullah *et al.*, "Organoids as an in vitro model of human development and disease," *Nat. Cell Biol.*, vol. 18, no. 3, pp. 246–254, Mar. 2016.

[9] M. A. Lancaster and M. Huch, "Disease modelling in human organoids," *Dis. Model. Mech.*, vol. 12, no. 7, Jul. 2019, Paper dmm039347.

[10] S. Haider *et al.*, "Self-Renewing trophoblast organoids recapitulate the developmental program of the early human placenta," *Stem Cell Rep.*, vol. 11, no. 2, pp. 537–551, Aug. 2018.

[11] M. Y. Turco *et al.*, "Trophoblast organoids as a model for maternal–fetal interactions during human placentation," *Nature*, vol. 564, no. 7735, pp. 263–267, Dec. 2018.

[12] C. E. Senner and M. Hemberger, "Regulation of early trophoblast differentiation - Lessons from the mouse," *Placenta*, vol. 31, no. 11, pp. 944–950, 2010.

[13] M. Knöfler *et al.*, "Human placenta and trophoblast development: Key molecular mechanisms and model systems," *Cell. Mol. Life Sci.*, vol. 76, no. 18, pp. 3479–3496, Sep. 2019.

[14] M. Horii *et al.*, "Human pluripotent stem cells as a model of trophoblast differentiation in both normal development and disease," *Proc. Nat. Acad. Sci. U. S. A.*, vol. 113, no. 27, pp. E3882–E3891, Jul. 2016.

[15] H. Okae *et al.*, "Derivation of human trophoblast stem cells," *Cell Stem Cell*, vol. 22, no. 1, pp. 50–63.e6, Jan. 2018.

[16] E. E. Capowski *et al.*, "Reproducibility and staging of 3D human retinal organoids across multiple pluripotent stem cell lines," *Development*, vol. 146, no. 1, Jan. 2019, Paper dev171686.

[17] J. F. Dekkers *et al.*, "High-resolution 3D imaging of fixed and cleared organoids," *Nat. Protoc.*, vol. 14, no. 6, pp. 1756–1771, Jun. 2019.

[18] I. Rakotoson *et al.*, "Fast 3-D imaging of brain organoids with a new single-objective planar-illumination two-photon microscope," *Front. Neuroanat.*, vol. 13, p. 77, Aug. 2019.

[19] S. Y. Jeong *et al.*, "Fabrication of dentin-pulp-like organoids using dental-pulp stem cells," *Cells*, vol. 9, no. 3, p. 642, Mar. 2020.

[20] A. W. Browne *et al.*, "Structural and functional characterization of human stem-cell-derived retinal organoids by live imaging," *Investig. Ophthalmol. Vis. Sci.*, vol. 58, no. 9, pp. 3311–3318, Jul. 2017.

[21] B. C. Chen *et al.*, "Lattice light-sheet microscopy: Imaging molecules to embryos at high spatiotemporal resolution," *Science*, vol. 346, no. 6208, Oct. 2014, Art. no. 1257998.

[22] A. F. Fercher *et al.*, "Measurement of intraocular optical distances using partially coherent laser light," *J. Mod. Opt.*, vol. 38, no. 7, pp. 1327–1333, 1991.
[23] D. Huang *et al.*, "Optical coherence tomography," *Science (80-.).*, vol. 254, no. 5035, pp. 1178–1181, 1991.
[24] W. Drexler *et al.*, "Optical coherence tomography today: Speed, contrast, and multimodality," *J. Biomed. Opt.*, vol. 19, no. 7, Jul. 2014, Art. no. 071412.
[25] M. Liu and W. Drexler, "Optical coherence tomography angiography and photoacoustic imaging in dermatology," *Photochem. Photobiol. Sci.*, vol. 18, no. 5, pp. 945–962, May 2019.
[26] Y. Jung *et al.*, "Longitudinal, label-free, quantitative tracking of cell death and viability in a 3D tumor model with OCT," *Sci. Rep.*, vol. 6, no. 1, pp. 1–11, Jun. 2016.
[27] M. Sharma *et al.*, "Imaging growth dynamics of tumour spheroids using optical coherence tomography," *Biotechnol. Lett.*, vol. 29, no. 2, pp. 273–278, Feb. 2007.
[28] Y. Huang *et al.*, "Longitudinal morphological and physiological monitoring of Three-dimensional tumor spheroids using optical coherence tomography," *J. Vis. Exp.*, no. 144, Feb. 2019.
[29] B. T. McLelland *et al.*, "Transplanted hESC-derived retina organoid sheets differentiate, integrate, and improve visual function in retinal degenerate rats," *Investig. Ophthalmol. Vis. Sci.*, vol. 59, no. 6, pp. 2586–2603, May 2018.
[30] R. K. Singh *et al.*, "Transplantation of human embryonic stem cell-derived retinal tissue in the subretinal space of the cat eye," *Stem Cells Dev.*, vol. 28, no. 17, pp. 1151–1166, Sep. 2019.
[31] L. Zhang *et al.*, "Oblique scanning laser microscopy for simultaneously volumetric structural and molecular imaging using only one raster scan," *Sci. Rep.*, vol. 7, no. 1, 2017, Art. no. 8591.
[32] R. Haindl *et al.*, "Ultra-high-resolution SD-OCM imaging with a compact polarization-aligned 840 nm broadband combined-SLED source," *Biomed. Opt. Express*, vol. 11, no. 6, Jun. 2020, Art. no. 3395.
[33] Y. Huang *et al.*, "Optical coherence tomography detects necrotic regions and volumetrically quantifies multicellular tumor spheroids," *Cancer Res.*, vol. 77, no. 21, pp. 6011–6020, Nov. 2017.
[34] R. Haindl *et al.*, "Three-beam doppler optical coherence tomography using a facet prism telescope and MEMS mirror for improved transversal resolution," *J. Mod. Opt.*, vol. 62, no. 21, pp. 1781–1788, Dec. 2015.
[35] P. Trencheav and M. Konopka, "Brief note: Combined haematoxylin, eosin and fluorescent stain for paraffin sections," *Pathology*, vol. 12, no. 1. pp. 79–81, 1980.
[36] J. M. Haggerty *et al.*, "Segmentation of epidermal tissue with histopathological damage in images of haematoxylin and eosin stained human skin," *BMC Med. Imag.*, vol. 14, no. 1, p. 7, Feb. 2014.
[37] L. Saleh *et al.*, "Evaluation of human first trimester decidual and telomerase-transformed endometrial stromal cells as model systems of in vitro decidualization," *Reprod. Biol. Endocrinol.*, vol. 9, p. 155, Dec. 2011.
[38] T. K. Koo and M. Y. Li, "A guideline of selecting and reporting intraclass correlation coefficients for reliability research," *J. Chiropr. Med.*, vol. 15, no. 2, pp. 155–163, Jun. 2016.
[39] J. M. Bland and D. G. Altman, "Statistical methods for assessing agreement between two methods of clinical measurement," *Lancet*, vol. 327, no. 8476, pp. 307–310, Feb. 1986.
[40] R. L. Schild *et al.*, "The kinase p38 regulates peroxisome proliferator activated receptor-γ in human trophoblasts," *Placenta*, vol. 27, no. 2–3, pp. 191–199, Feb. 2006.
[41] G. Meinhardt *et al.*, "Pivotal role of the transcriptional co-activator YAP in trophoblast stemness of the developing human placenta," *Proc. Nat. Acad. Sci. U. S. A.*, vol. 117, no. 24, pp. 13562–13570, Jun. 2020.
[42] S. Tang *et al.*, "Imaging subcellular scattering contrast by using combined optical coherence and multiphoton microscopy," *Opt. Lett.*, vol. 32, no. 5, pp. 503–505, Mar. 2007.
[43] E. D. Johnstone *et al.*, "Epidermal growth factor stimulation of trophoblast differentiation requires MAPK11/14 (p38 MAP kinase) activation," *Biol. Reprod.*, vol. 73, no. 6, pp. 1282–1288, Dec. 2005.
[44] G. Daoud *et al.*, "ERK 1/2 and p38 regulate trophoblasts differentiation in human term placenta," *J. Physiol.*, vol. 566, no. 2, pp. 409–423, Jul. 2005.
[45] V. Jokimaa *et al.*, "Expression of syndecan-1 in human placenta and decidua," *Placenta*, vol. 19, no. 2–3, pp. 157–163, 1998.
[46] S. Dahl-Jensen and A. Grapin-Botton, "The physics of organoids: A biophysical approach to understanding organogenesis," *Development*, vol. 144, no. 6, pp. 946–951, Mar. 2017.
[47] A. L. Oldenburg *et al.*, "Inverse-power-law behavior of cellular motility reveals stromal-epithelial cell interactions in 3D co-culture by OCT fluctuation spectroscopy," *Optica*, vol. 2, no. 10, pp. 877–885, Oct. 2015.
[48] L. Yang *et al.*, "Characterizing optical coherence tomography speckle fluctuation spectra of mammary organoids during suppression of intracellular motility," quant. *Imag. Med. Surg.*, vol. 10, no. 1, pp. 76–85, Jan. 2020.